Supporting information

Microbatteries with twin-Swiss-rolls redefine performance limits in the sub-square millimeter range

Yang Li,[abc] Minshen Zhu,*[ac] Dmitriy D. Karnaushenko,[a] Fei Li,[abc] Jiang Qu,[abc] Jinhui Wang,[abc] Panpan Zhang,[d] Lixiang Liu,[c] Rachappa Ravishankar,[c] Vineeth Kumar Bandari,[abc] Hongmei Tang,[bc] Zhe Qu,[bc] Feng Zhu,*[abce] Qunhong Weng,*[cf] Oliver G. Schmidt*[abcg]

[a]Center for Materials, Architectures and Integration of Nanomembranes (MAIN), Chemnitz University of Technology, Chemnitz 09126, Germany.

[b]Material Systems for Nanoelectronics, Chemnitz University of Technology, Chemnitz 09107, Germany.

[c]Institute for Integrative Nanosciences, Leibniz IFW Dresden, Dresden 01069, Germany.

[d] State Key Laboratory of Materials Processing and Die & Mould Technology, School of Materials Science and Engineering, Huazhong University of Science and Technology, Wuhan 430074, China.

[e]State Key Laboratory of Polymer Physics and Chemistry, Changchun Institute of Applied Chemistry, Chinese Academy of Sciences, Changchun 130022, China.

[f]School of Materials Science and Engineering, Hunan University, Changsha 110016, China.

[g]School of Science, Dresden University of Technology, Dresden 01069, Germany.

Experimental procedures

The fabrication of Swiss-roll microbattery: The Swiss-roll microelectrodes were fabricated by employing micro-origami technology. The photoresist (AZ5214E, Microchemicals) was patterned as a sacrificial layer by a mask-less aligner (Heidelberg MLA100). Then, Ti and Au layers were deposited on the sacrificial layer by electron-beam (e-beam) evaporation (Plassy deposition machine) at a high vacuum of 4×10^{-7} bar. Then 100 nm Ti layer was deposited between the Swiss-roll electrode and contact pad with photolithography and sputtering deposition process. The Ti/Au layer rolled up from the substrate after etching away the sacrificial layer by acetone. The Swiss-roll in different diameters were fabricated with tuning thicknesses of strain layer (60 nm (Ti (30 nm)/Au (30 nm)), 80 nm (Ti (40 nm)/Au (40 nm)), and 100 nm (Ti (50 nm)/Au (50 nm))) (Fig. S1).

After the formation of twin Swiss-roll microelectrodes, Zn and MnO_2 are deposited into the micro-scaffolds by electrochemical deposition. The aqueous solution of $Mn(CH_3COO)_2 \cdot 4H_2O$ (0.1 mol L^{-1}) and Na_2SO_4 (0.1 mol L^{-1}) was used as the electrolyte for MnO_2 deposition. The deposition was conducted at the constant potential of 1 V by using platinum wire and Ag/AgCl (saturated KCl) as the counter and the reference electrode, respectively. Zn was deposited on the microanode. The electrodeposition was conducted at a constant current density of -20 mA cm^{-2} for 10 min in the mixture (50 mL) of $ZnSO_4 \cdot 7H_2O$ (0.5 mol L^{-1}), Na_2SO_4 (0.75 mol L^{-1}), and H_3BO_3 (0.3 mol L^{-1}).

The Swiss-roll microbattery was encapsulated with SU8 photoresist by using photolithograph technology (Fig. S11). After the rolling-up of twin Swiss-roll, the device was dried at room temperature for several min. SU8-25 was spin-coated on the dried device at 1,000 rpm for 60 s. After soft baking at 65 °C for 5 min and at 95 °C for 5 min, the samples were exposed to UV light (365 nm, 1500 mJ/cm^2) using MLA 100 maskless aligner. After hard baking at 65 °C for 1 min and at 95 °C for 3 min, the samples were developed in PGMEA for 6 min and rinsed in acetone for 90 seconds to remove unexposed SU-8 photoresist. Then the active materials were deposited into the twin Swiss-roll. After that, one drop of electrolyte was injected into the SU8 box. A piece of SU8 was covered on the top of the SU8 box to complete the encapsulation of the Swiss-roll microbattery (Fig. S7).

Morphological and structural characterization: X-ray diffraction (XRD) (Co Ka radiation (λ = 1.5418 Å), X'Pert PRO MPD, Philips) was used to analyze the material structures and

compositions. The Raman spectroscopy was performed using the Raman microscope with a laser wavelength of 442 nm (LabRAM HR Evolution, HORIBA Scientific). The morphologies of materials and devices were observed using a field-emission scanning electron microscope (FIB-SEM, Zeiss NVision 40, Germany).

Electrochemical characterization: Cyclic voltammogram (CV) curves were measured by an electrochemical workstation (MULTIAUTOLAB/M101, Metrohm Autolab). The galvanostatic charge-discharge measurements were taken on a multichannel battery-testing system (Arbin BT 2000). The footprint areas of two Swiss-roll microelectrodes were used to calculate the current density, areal capacity, and energy density. All those measurements were obtained at room temperature in an open-air condition. The solution containing $Zn(CF_3SO_3)_2$ (3 mol L^{-1}) and $Mn(CF_3SO_3)_2$ (0.025 mol L^{-1}) was utilized as the electrolyte for microbatteries with different deposition time (1 min, 2 min, and 4 min) of MnO_2. The solution containing $Zn(CF_3SO_3)_2$ (3 mol L^{-1}) and $Mn(CF_3SO_3)_2$ (0.1 mol L^{-1}) was utilized as the electrolyte for microbatteries with different deposition time (6 min, and 7 min) of MnO_2. The weight of a Swiss-roll electrode is averaged by the mass of 100 Swiss-roll electrodes (Fig. S12) as one single Swiss-roll electrode is too light to measure. The average weight of one MnO_2 and Zn loaded onto Swiss-roll electrodes are only 0.8 and 2.3 μg, respectively (the mass of one Ti/Au Swiss-roll is 0.08 μg).

The footprint area for electrodes are areas covered by two Swiss-roll electrodes (0.5 mm × 0.045 mm × 2). The footprint area in performance calculation for the packaged microbattery uses the overall dimension (Figure S13, 0.6 mm × 0.19 mm). The volume used to calculate the volumetric capacity and energy density excludes the thickness of the substrate (Figure S13, 0.6 mm × 0.19 mm × 0.15 mm). The weight of MnO_2 is measured by averaging the weights of 100 MnO_2 Swiss-roll microelectrodes because it is difficult to get an accurate value for a single MnO_2 Swiss-roll microelectrode.

The footprint energy density of the Swiss-roll microbattery is calculated using the equations:

$$E_A = \int_0^t IV(t)dt / A_{TR}$$

Where V(t) is the voltage during the discharge process.

The volumetric energy density of the encapsulated Swiss-roll microbattery is calculated using the equations:

$$E_V = \int_0^t IV(t)dt/V$$

FEM simulations: Ansys 17.2 mechanical academics was used for FEM simulations. The bilayer model consisted of Ti (30 nm) and Au (30 nm). The lateral size of the model was set to 48 × 48 μm. Deformable remote displacement with zero rotational and displacing components was applied at the end of the rolled-up structure to stabilize simulation over wide variety of parameters. L and k were introduced to investigate the effect of these parameters on the Swiss-roll. Mechanical isotropic elasticity of materials for FEM simulations were derived from the Young's modulus and the Poisson's ratio of materials. Young's modulus and Poisson's ratio of Au are 77 GPa and 0.42, respectively. For Ti, these values were 96 GPa and 0.36, respectively. Assembling process of the Ti/Au bilayer was performed using static structural analysis. Stress in materials was generated by manipulating artificial coefficients of thermal expansion and thermal boundary conditions. The parametric calculations were firstly fit to the experiment-obtained diameter of the tube without holes. Thermal boundary conditions were set as -0.3 °C for the Au layer and 0.3 °C for the Ti layer. All thermal conditions were uniformly incremented over 500 steps from 0 °C up to the final temperature. The static module for solver controls was enabled a large deflection option.

Mechanical measurement:

The mechanical measurement was performed by AFM (Dimension Icon, Bruker USA) in contact mode with a probe (OMCL-AC160TS-R3) of spring constant 26 N/m. The cantilever tip view is shaped like a sharpened tetrahedral with a tip radius of 8-12 nm and a half-open angle of the cone is ~9°. It is made from highly doped silicon to dissipate the static charge and offer a high mechanical Q-factor for large sensitivity. The mechanical measurements are done at the three different positions of Swiss-rolls with a feature set stage reference panel to set origin (X=0 ,Y=0) point for one of the corners of the square sample. The position sensitive photo-detector sensitivity S (nm/V) is calibrated by measuring the force curve on a silicon surface, which was considered infinitely stiff with respect to a low spring constant cantilever. The cantilever spring constant k (nN/nm) was determined by thermal tuning[1].

The vertical loading force F (nN) was applied on the Swiss-roll surface and where $^{\Delta d_V}$ is a change in the photodiode voltage due to cantilever deflection given in equation (1)[2].

$$F = kS\Delta d_V \quad (1)$$

The tip-sample separation distance D (nm) is estimated by subtracting cantilever deflection $S\Delta d_V$ from the change in *z*-piezo displacement Δz (nm)[2]

$D = \Delta z - S\Delta d_V$ (2)

The Hertz model which describes purely elastic deformation of spherical bodies in contact has been used to calculate Young's modulus (E_s) of Swiss-rolls from the force-indentation curve.

$$F = \frac{4}{3} E_r \sqrt{R\delta^3} \quad (3)$$

$$E_r = \left(\frac{1 - \vartheta_s^2}{E_s} + \frac{1 - \vartheta_{tip}^2}{E_{tip}} \right)^{-1} \quad (4)$$

We assume that the tip modulus E_{tip} is infinitely large compared to the sample and Poisson's ratio of tip ϑ_{tip} and R (nm) is the apex radius of the tip by assuming Poisson's ratio of sample is ϑ_s Young's modulus of the sample E_s is calculated and a result of the fit is a reduced modulus E_r. The morphology and Young's modulus of Swiss-rolls were analyzed analysis in NanoScope Analysis software (V1.80, Bruker, USA).

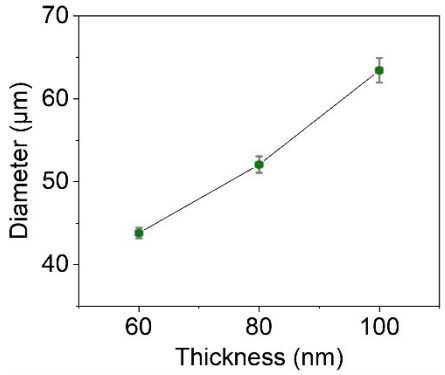

Fig. S1. Diameter of Swiss rolls as a function of the thickness of the Ti and Au bilayer (Ti/Au).

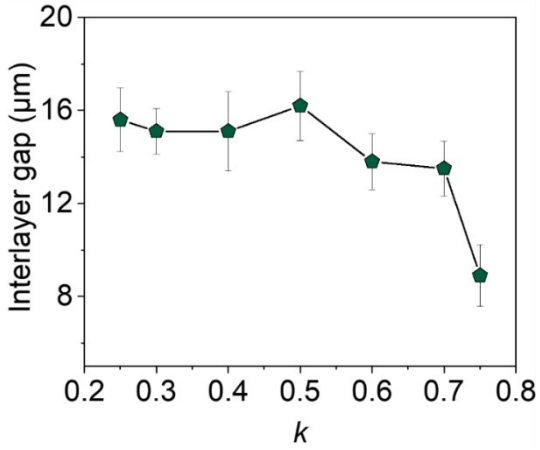

Fig. S2. The total interlayer gap of the Swiss-roll-multiple as a function of *k*. The total interlayer gap is the diameter difference between Swiss-roll-single and Swiss-roll-multiple at same *k* value.

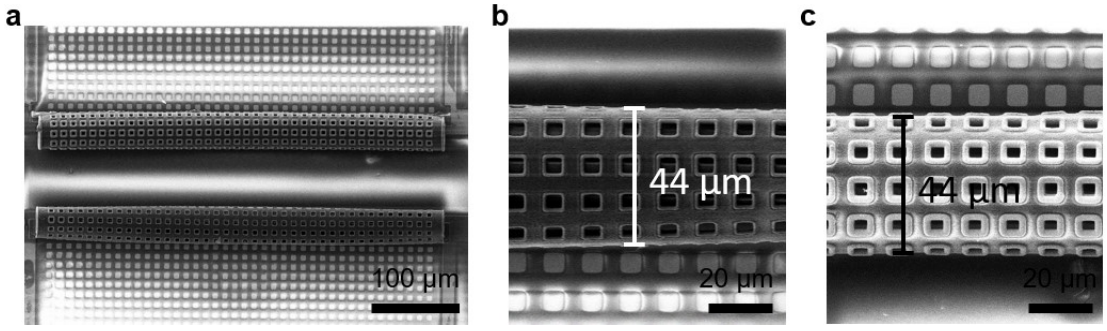

Fig. S3. SEM images of (a) twin Swiss rolls loaded with Zn and MnO_2. Magnified SEM images of (b) Zn and (c) MnO_2 Swiss-roll microelectrode.

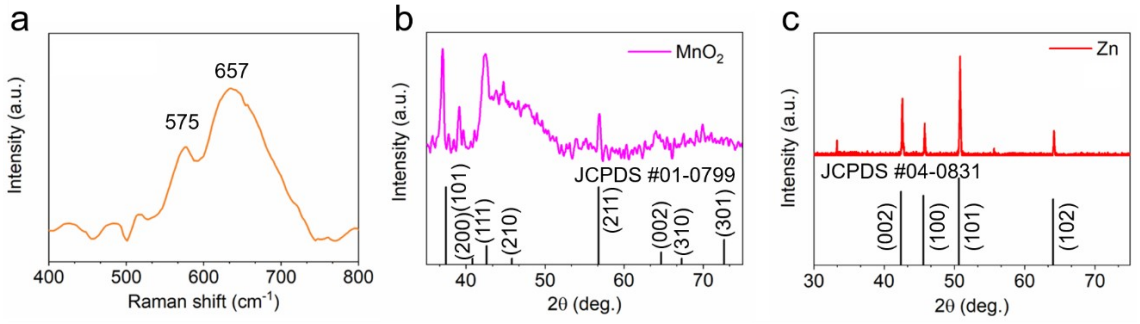

Fig. S4. (a) Raman spectrum of electrochemically deposited MnO_2. XRD patterns of the deposited MnO_2 (b) and Zn (c).

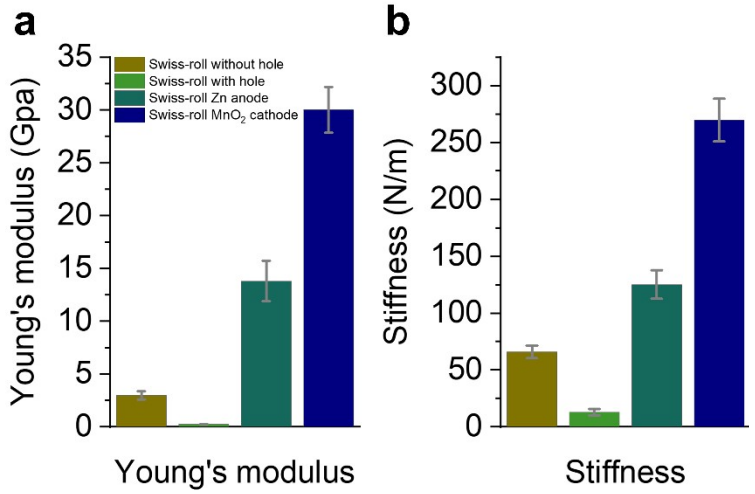

Fig. S5. Mechanical property of the Swiss-rolls: (a)Young's modulus; (b)Stiffness.

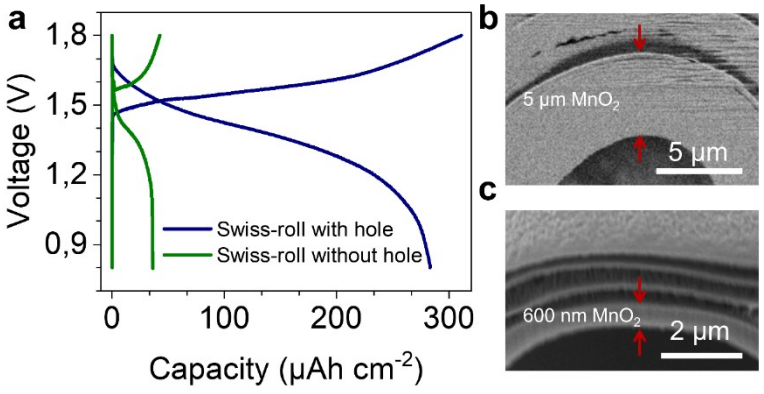

Fig. S6. (a) Charge and discharge curves of the microbatteries with and without holes at a current density of 500 μA cm^{-2}. The SEM images of the cross-section of MnO_2 Swiss-roll microelectrode with (b) and without holes (c) at the same deposition time of MnO_2 (7 min).

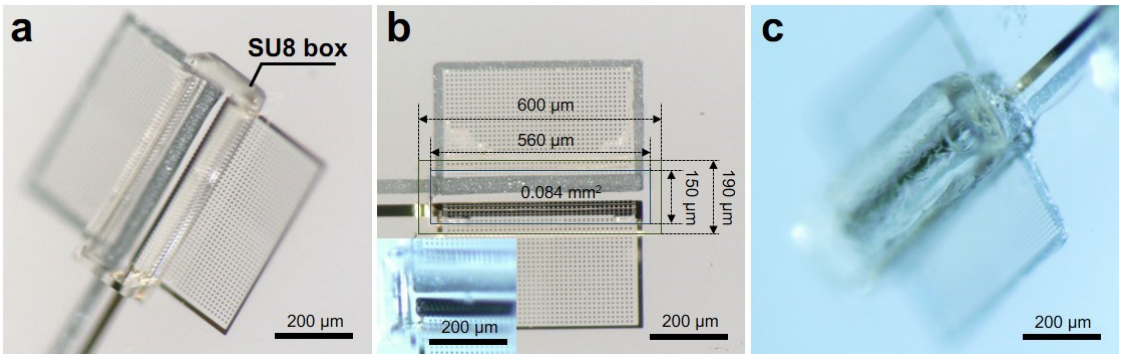

Fig. S7. Images of the SU8 box patterned around twin Swiss-roll microelectrodes: (a) perspective view, (b) top view with labeled dimensions (The inset in (b) shows the Swiss-roll microelectrodes), and (c) after filling the electrolyte.

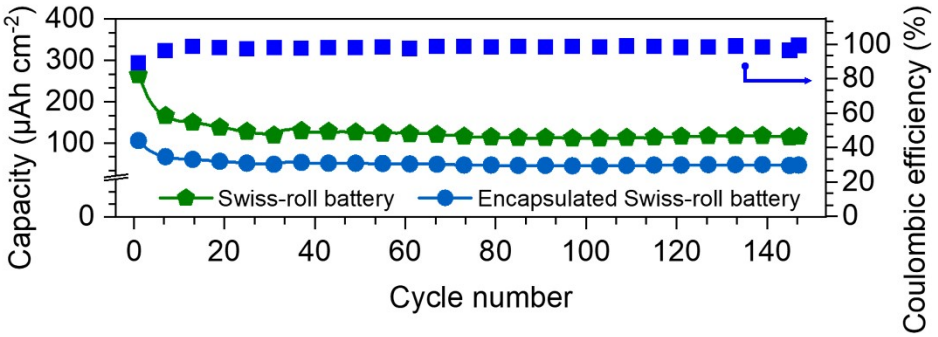

Fig. S8. Cycling performance of Swiss-roll microbattery and encapsulated Swiss-roll microbattery at a current density of 500 μA cm^{-2}.

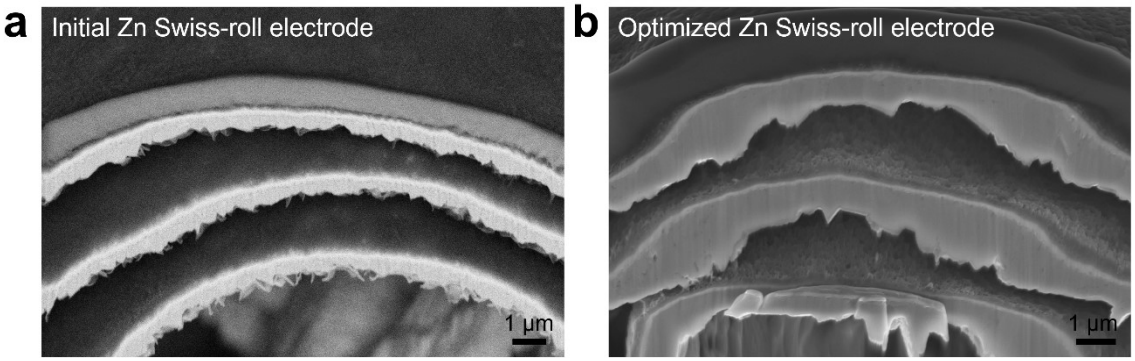

Fig. S9. (a) Cross-section of Swiss-roll Zn microelectrode with 5 min deposition. (b) Cross-section of Swiss-roll Zn microelectrode with 10 min deposition.

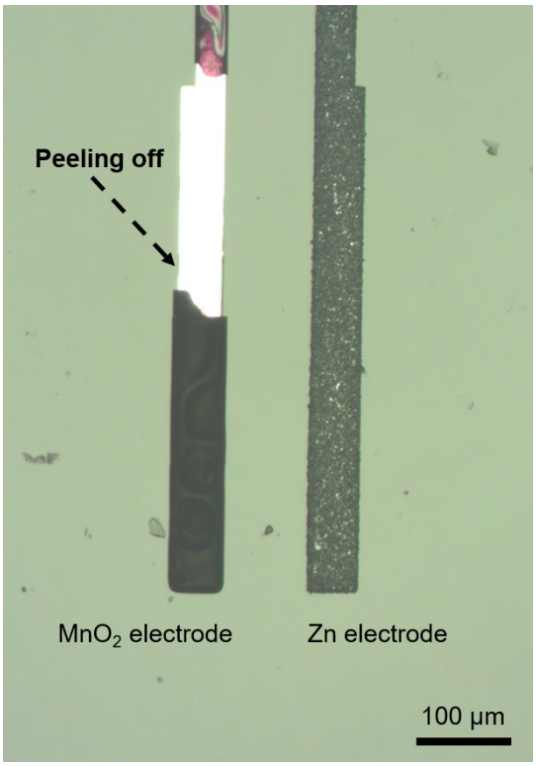

Fig. S10. Optical image of a planar Zn-MnO_2 battery after cycling.

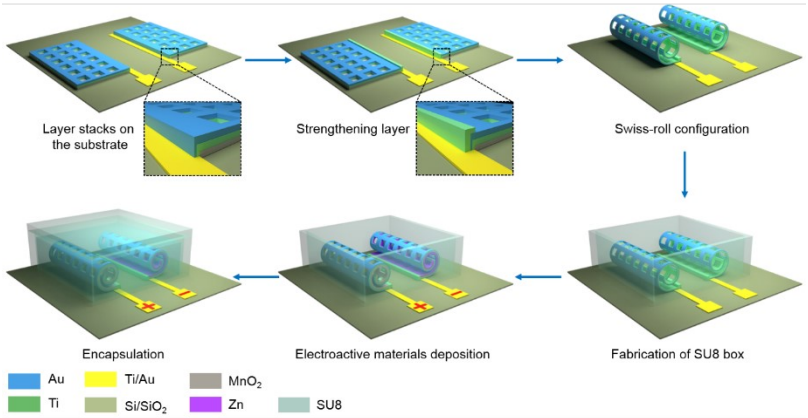

Fig. S11. Schematic of the fabrication process of the encapsulated Swiss-roll microbattery.

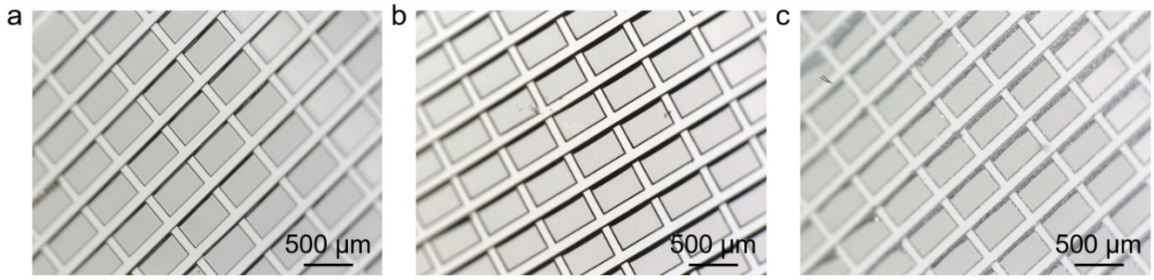

Fig. S12. Optical microscopy images of (a) bare Swiss-roll microelectrodes, (b) MnO_2 Swiss-roll microelectrodes and (c) Zn Swills-roll microelectrodes.

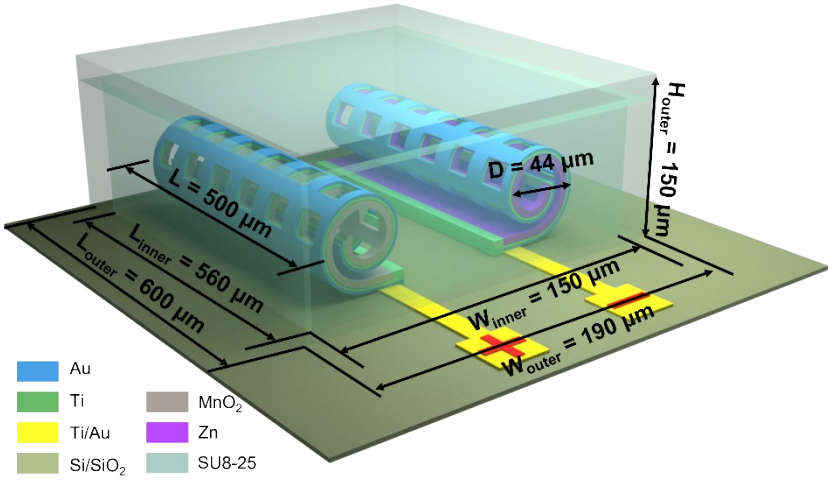

Fig. S13. Schematic of the dimensions of the packaged cell.

Table S1. Performance comparison of various aqueous rechargeable batteries.

Cathode materials	Electrolyte	Capacity (mAh g^{-1})	Energy density (mWh g^{-1})	Ref.
MnO_2	1 mol L^{-1} $ZnSO_4$	233	–	3
MnO_2	3 mol L^{-1} $Zn(CF_3SO_3)_2$ + 0.1 mol L^{-1} $Mn(CF_3SO_3)_2$	258	254	4
Mn_2O_3	2 mol L^{-1} $ZnSO_4$ + 0.1 mol L^{-1} $MnSO_4$	148	–	5
Mn_3O_4	2 mol L^{-1} $ZnSO_4$ + 0.1 mol L^{-1} $MnSO_4$	296	–	6
$ZnMn_2O_4$	1 mol L^{-1} $ZnSO_4$ + 0.05 mol L^{-1} $MnSO_4$	120	–	7
$LiMn_2O_4$	1 mol L^{-1} $Zn(TFSI)_2$ + 20 mol L^{-1} LiTFSI	66	180	8
MnO_2	**3 mol L^{-1} $Zn(CF_3SO_3)_2$ + 0.1 mol L^{-1} $Mn(CF_3SO_3)_2$**	**194**	**257**	**This work**

Reference:

1 J. L. Hutter and J. Bechhoefer, *Rev. Sci. Instrum.*, 1993, **64**, 1868-1873.

2 B. Liu and J. Fu, *J. Micromechanics Microengineering*, 2015, **25**, 065006.

3 M. H. Alfaruqi, J. Gim, S. Kim, J. Song, J. Jo, S. Kim, V. Mathew and J. Kim, *J. Power Sources*, 2015, **288**, 320-327.

4 H. L. Pan, Y. Y. Shao, P. F. Yan, Y. W. Cheng, K. S. Han, Z. M. Nie, C. M. Wang, J. H. Yang, X. L. Li, P. Bhattacharya, K. T. Mueller and J. Liu, *Nat. Mater.*, 2016, **1**, 16039.

5 B. Z. Jiang, C. J. Xu, C. L. Wu, L. B. Dong, J. Li and F. Y. Kang, *Electrochim. Acta.*, 2017, **229**, 422-428.

6 C. Y. Zhu, G. Z. Fang, J. Zhou, J. H. Guo, Z. Q. Wang, C. Wang, J. Y. Li, Y. Tang and S. Q. Liang, *J. Mater. Chem. A*, 2018, **6**, 9677-9683.

7 X. W. Wu, Y. H. Xiang, Q. J. Peng, X. S. Wu, Y. H. Li, F. Tang, R. C. Song, Z. X. Liu, Z. Q. He and X. M. Wu, *J. Mater. Chem. A*, 2017, **5**, 17990-17997.

8 F. Wang, O. Borodin, T. Gao, X. L. Fan, W. Sun, F. D. Han, A. Faraone, J. A. Dura, K. Xu and C. S. Wang, *Nat. Mater.*, 2018, **17**, 543-549.